Cell Mechanics Studied by a Reconstituted Model Tissue

Tetsuro Wakatsuki,* Michael S. Kolodney,† George I. Zahalak,‡ and Elliot L. Elson*

*Department of Biochemistry and Molecular Biophysics, Washington University School of Medicine, St. Louis, Missouri 63110; †Division of Dermatology, Department of Medicine, 1519 MacDonald Research Laboratory, UCLA School of Medicine, Los Angeles, California 90095; and ‡Departments of Biomedical and Mechanical Engineering, School of Engineering, Washington University, St. Louis, Missouri 63130 USA

ABSTRACT Tissue models reconstituted from cells and extracellular matrix (ECM) simulate natural tissues. Cytoskeletal and matrix proteins govern the force exerted by a tissue and its stiffness. Cells regulate cytoskeletal structure and remodel ECM to produce mechanical changes during tissue development and wound healing. Characterization and control of mechanical properties of reconstituted tissues are essential for tissue engineering applications. We have quantitatively characterized mechanical properties of connective tissue models, fibroblast-populated matrices (FPMs), via uniaxial stretch measurements. FPMs resemble natural tissues in their exponential dependence of stress on strain and linear dependence of stiffness on force at a given strain. Activating cellular contractile forces by calf serum and disrupting F-actin by cytochalasin D yield "active" and "passive" components, which respectively emphasize cellular and matrix mechanical contributions. The strain-dependent stress and elastic modulus of the active component were independent of cell density above a threshold density. The same quantities for the passive component increased with cell number due to compression and reorganization of the matrix by the cells.

INTRODUCTION

Tissue models reconstituted from specified cells and extracellular matrix (ECM) components provide simplified biological systems in which to study cell-matrix interactions in wound healing and tissue development (Bell et al., 1979, Grinnell, 1994). Quantitative measurements of the force exerted by these models provide a powerful and flexible approach to study mechanisms of force regulation in nonmuscle cells (Goeckeler and Wysolmerski, 1995; Kolodney and Elson, 1993, 1995; Kolodney and Wysolmerski, 1992). Measurements of tissue stiffness introduce an additional dimension, revealing mechanical functions of matrix components and cellular structural systems such as the cytoskeleton. Stiffness measurements can also probe mechanical interactions between cells and ECM, and mechanisms of tissue remodeling in development and wound healing. Moreover, characterization and control of the mechanical properties and functions of reconstituted tissue equivalents are essential tasks for practical applications of tissue engineering.

We have developed methods for quantitative measurement of the forces produced by reconstituted tissue models both of nonmuscle cells and cardiomyocytes (Eschenhagen et al., 1997; Kolodney and Elson, 1993). This paper describes an extension of this method to measurements of tissue stiffness and a characterization of the mechanical properties of reconstituted tissue models assembled with chick embryo fibroblasts. One of our long-range goals is to use reconstituted tissue models to study the mechanical functions of cytoskeletal proteins. Because the cells, the matrix, and their interactions determine the mechanical properties of model tissues, we have sought conditions in which cytoskeletal contributions to the mechanics can be measured specifically.

A major conclusion from this work is that under specified conditions, the mechanical contributions of the cells to the fibroblast-populated matrix (FPM) can be distinguished from those of the matrix. The stiffness of the model tissues is the sum of two components, termed "Active" and "Passive." The latter represents the mechanical properties of FPMs from which cytoskeletal and some matrix contributions have been eliminated by disrupting actin filaments. The ECM dominates the Passive component. The Active and Passive components have significantly different mechanical properties. The dynamic stiffness increases much more rapidly at high strain for the passive than for the active component. The force that resists stretching the matrix is an exponential function of the strain. At high strain, at which the matrix dominates the mechanical properties of the FPM, the dynamic stiffness of the tissue is therefore a linear function of the force that the tissue exerts or which is exerted on the tissue. Furthermore, the dynamic stiffness of the tissue model increases linearly with the logarithm of the oscillation frequency at which it is stretched. Both these properties are seen in natural biological tissues (Fung, 1993). They present a challenge for structural interpretation.

Received for publication 28 February 2000 and in final form 31 July 2000.

Address reprint requests to Dr. Elliot L. Elson, Dept. of Biochemistry/Molecular Biophysics, Washington University School of Medicine, 600 S. Euclid Ave., Box 8231, St. Louis, MO 63110-1093. Tel.: 314-362-3346; Fax: 314-362-7183; E-mail: elson@biochem.wustl.edu.

0006-3495/00/11/2353/16 $2.00

MATERIALS AND METHODS

Cell and tissue culture

Chicken embryo fibroblasts (CEFs) isolated from 11-day chicken embryos (Spafas Inc., Preston, CT) were maintained in Dulbecco's modified Eagle's medium (DMEM) supplemented with 10% fetal calf serum (FCS), peni-

cillin at 50 units/ml, and streptomycin at 50 mg/ml. The CEFs used to make FPMs were passaged once or twice from primary cultures. Monomeric collagen solubilized in 0.02 M acetic acid (Upstate Biotechnology Inc., Lake Placid, NY) was neutralized at 4°C with 0.1 N NaOH and mixed with concentrated DMEM stock to yield a final normal DMEM concentration. The fibroblasts suspended by trypsin (Fig. 1 *a*) were mixed with the collagen solution (Fig. 1 *b*), the cell suspension was poured into Teflon casting wells (Fig. 1 *c*), and wells were incubated at 37°C with 5% CO_2 (Fig. 1 *d*). The collagen polymerized within 15–30 min and fibroblasts were captured within the hydrated collagen gel. The collagen gel formed a ring (3 mm thick, 3 cm diameter) between the inner wall of the cylindrical well and the central mandrel. While in culture the cells compressed this ring, reducing its volume ~10-fold (thickness 200–300 μm). The ring could then be removed from the mandrel (Fig. 1, *e* and *f*) and mounted on the measuring instrument (Fig. 1 *g*) as described below.

Mechanical measurements

After 2 days of incubation (serum starvation for the final 12–16 h), the mandrel was removed from the well and the FPM-ring was removed gently from the mandrel. The FPM-ring was looped over the triangular hook connected to an isometric force transducer (model 52-9545, Harvard Apparatus, South Natick, MA) by a gold chain. The ring was also looped over a horizontal bar connected to a sliding element moved linearly by a stepper motor (P/N 1-19-3400 24V DC 1.8° step size, Haward Industry, St. Louis, MO) controlled by a microstepping driver (IM483 Intelligent Motion Systems, Inc., Marlborough CT) (Fig. 1 *g*). The apparatus changes the tissue length with prescribed time and amplitude to measure stress and dynamic modulus of the sample. The microstepping driver controlled by a personal computer with custom software (developed by Bill McConnaughey) enabled the stepper motor to achieve smooth motion. An analog-to-digital signal converter (CIO-DAS1602/16, Computer Boards, Inc., Mansfield, MA) attached to the computer translated the voltage signal from the isometric force transducer to a digital signal for recording. The sample was submerged in 50 ml Hepes-buffered DMEM (pH 7.4) in a thermoregulated organ bath (Harvard Apparatus, South Natick, MA) maintained at 37°C. The two horizontal bars over which the ring was looped were initially set to hold the ring at its original contour length (corresponding to [½] of the circumference of the mandrel). The amplitude of the force response divided by the driving amplitude corresponded to the dynamic stiffness of the sample subjected to a sinusoidal length change (20 μm amplitude; <0.5% stain, 0.5 Hz frequency). The dynamic stiffness and tension of the FPM were measured at various strain levels by elongating and shortening the sample at a constant rate (10 μm/min) up to 20% strain.

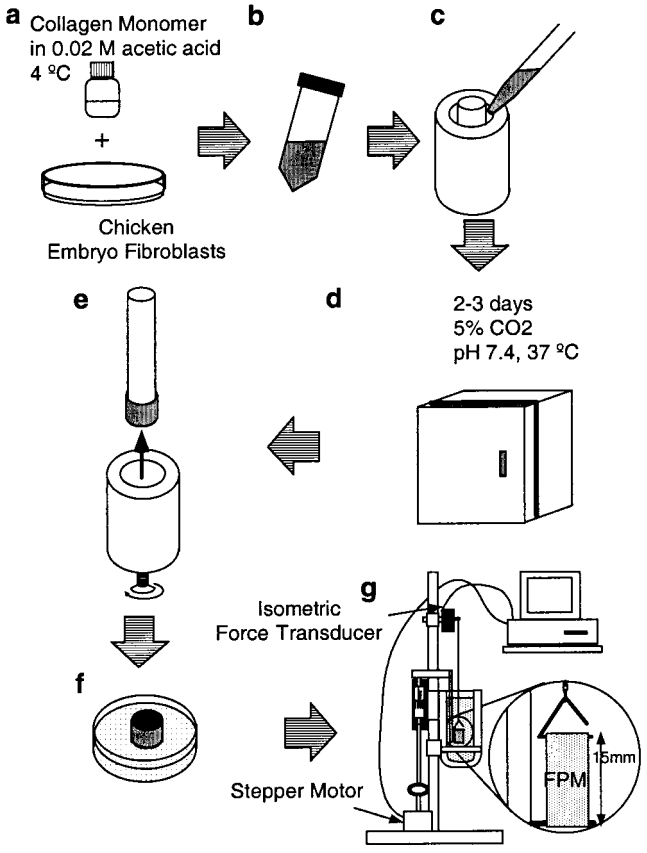

FIGURE 1 Schematic of methods for preparing and measuring FPMs. The CEFs and monomeric collagen (*a*) are mixed in DMEM at pH 7 (*b*). This solution is poured into casting wells (*c*) and polymerized at 37°C (*d*). The wells are incubated (*d*) for few days, during which the cells compress and remodel the collagen matrix. After the incubation the mandrel is removed from the well (*e*) and the FPM-ring is removed gently from the mandrel (*f*). The FPM-ring is connected to the force-measuring apparatus (an isometric force transducer) and a stepper motor that controls the tissue strain (*g*).

Measurement of tissue cross-sectional area

After a 2-day incubation the FPM forms a tight ring around the mandrel. The mandrel with the FPM was placed vertically on an inverted microscope (IM-35, Carl Zeiss Inc., Thornwood, NY). An image of the ring viewed along its axis was captured by video camera and the thickness was determined by image analysis. The width of the FPM was measured using a caliper.

Estimation of cross-sectional areas

The cells in the FPMs were stained with the cytoplasmic fluorescent dye Cell Tracker (Molecular Probes, Eugene, OR) using the recommended concentration in serum-free DMEM and incubating for 15 min at 37°C. The samples were washed twice with PBS to remove excess dye and fixed with 3.7% formaldehyde in PBS for 30 min at room temperature. The circumferential direction of the FPM was aligned to the *y* axis of the confocal scanning axis so that the *y* axis of the image was always parallel to the direction of stretch. A total of 36 images were taken at focal planes separated by 2 μm along the *z* axis of the FPM (perpendicular to its planar surface). The smallest confocal aperture (0.7 mm) was used to maximize resolution along the *z* axis, and the parameters were carefully chosen to use the whole intensity range and to avoid saturation. A stack of 36 images was resliced in the plane perpendicular to the axis of the stretch by ScionImage software (Scion Corporation, Frederick, MD). The total cross-sectional area of cells was computed by summing all the pixels with intensity higher than a threshold. The threshold was determined once using one of the images following a published procedure (Satoh et al., 1996). The same threshold was used for all the samples because the images were obtained using the same confocal parameters. The accuracy and reproducibility of the reslicing was confirmed by repeating the procedure for spherical fluorescent beads (6 μm diameter) embedded in a collagen matrix.

RESULTS

A remodeling of the matrix by the cells strongly influences the mechanical characteristics of an FPM. After gelation of the collagen, the cells adhere to the collagen fibers, elon-

gate, and compress and stiffen the collagen matrix, reducing its volume by ~10-fold and increasing its stiffness from near zero to ~1 dyn/μm. The cells near the edge of the tissue orient parallel to the edge (Kolodney and Elson, 1993). The elongated shapes of the cells labeled with a fluorescent cytoplasmic dye and their distribution within the matrix are readily displayed using scanning confocal fluorescence microscopy (Fig. 2). The mechanical properties of tissues depend on the distribution of the cells and their orientations. To a reasonable first approximation we may consider the positions and orientations of the cells to be random (except near the edges of the tissue). See Zahalak et al. (2000) (accompanying paper) for a more detailed discussion of orientation effects.

Our major purpose in this work is to characterize the relative contributions of the cells and the matrix to the mechanical properties of the reconstituted model tissues. To accomplish this goal we measured the stiffness of the FPMs at various strains and strain rates. We have developed an instrument to measure the forces either generated by an FPM or applied to it by a computer-controlled microstepping motor (Fig. 1). Using this instrument we can measure stiffness of a model tissue by determining the force required to stretch it to a defined level of strain. As described above, we have typically used a triangular ramp stretch on which is superimposed a small sinusoidal strain (ν = 0.5 Hz). The dynamic stiffness was measured as the peak-to-peak change in force per change in strain.

Dependence of force and stiffness on slow strain

Typically, the model tissue is subjected to a sequence of stretch cycles. In each cycle it is slowly stretched from 0 to 20% over 30 min and is then returned at the same rate to its original length. The increase in force during the first stretch is substantially larger than in subsequent stretches (Fig. 3). This change in mechanical properties during the first cycle is not affected by disrupting the organization of cellular actin filaments with cytochalasin D (CD), and so is most likely due to a change in the properties of the matrix during the first stretch (Asnes and Wakatsuki, unpublished observations). For each stretch after the first there is a further small decrease in maximum force. We have chosen to use only the first loading cycle for "preconditioning" because the major irreversible change in tissue mechanical proper-

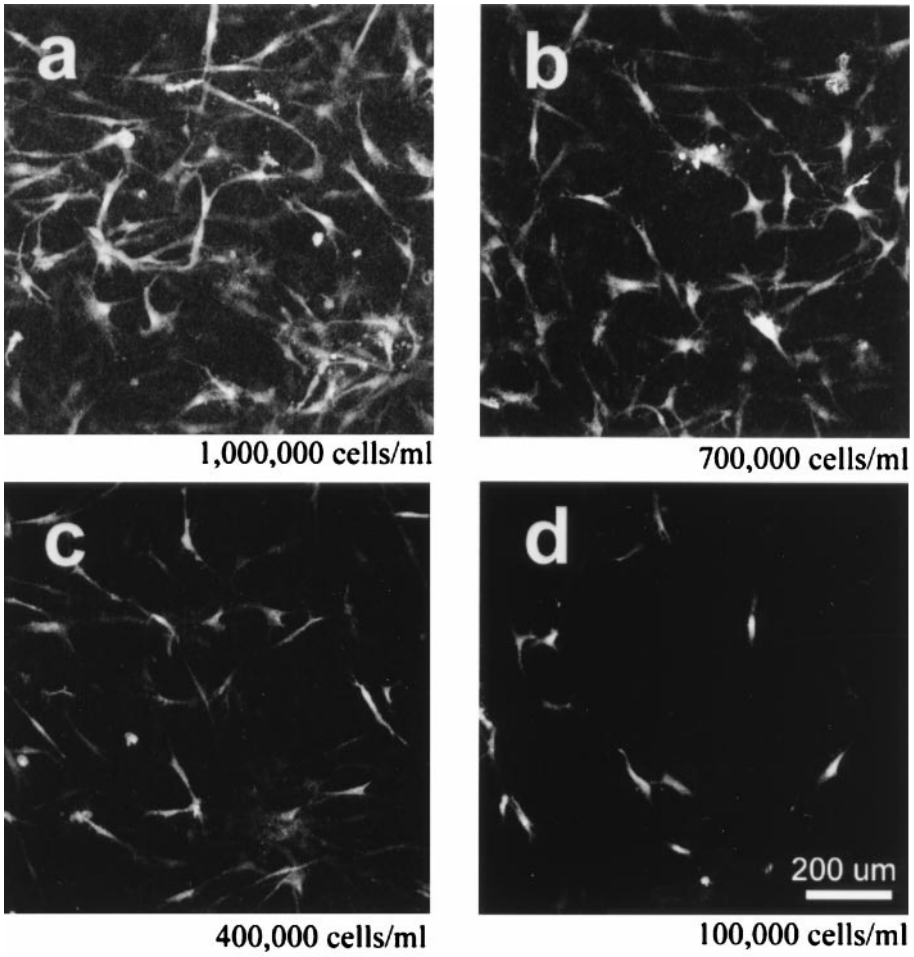

FIGURE 2 Scanning confocal micrographs of FPMs with different concentrations of cells. The fibroblasts were labeled with a fluorescent cytoplasmic dye (Cell Tracker). The cells are elongated and randomly oriented. The concentrations of fibroblasts before gel compression were 1,000,000 (*a*), 700,000 (*b*), 400,000 (*c*), and 100,000 (*d*) cells per initial unit volume (1 ml) of the cell-collagen solution.

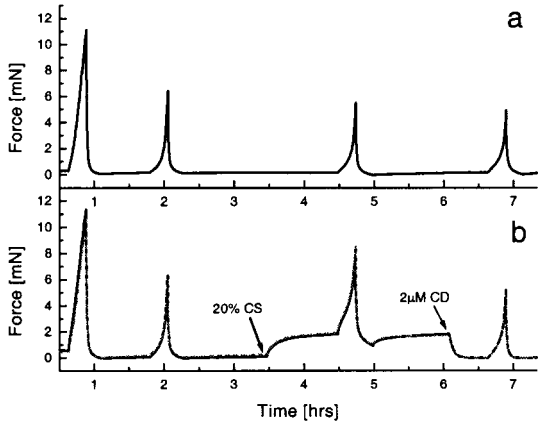

FIGURE 3 Force response to stretch. Typical force responses from a sequence of 4 stretch cycles applied to one FPM were traced in time. The first stretch cycle produces a substantially larger peak force than the subsequent cycles. A much smaller (~6%) reduction in peak force is seen in each of the subsequent cycles (*a*). Panel *b* illustrates the reproducibility of the measurements by showing force responses of duplicate FPMs (*solid line* and *gray broken line*). The effects of both 20% calf serum (increase in contractility) and 2 μM CD (abolition of active contractility) are almost identical in the duplicates. The cycle time was set to 30 instead of 60 min for this experiment to accommodate the additional experimental manipulations. The force-strain and stiffness-strain curves from two different cycle times, however, are almost identical.

ties occurs during this stretch. Moreover, the small changes that occur between the subsequent stretch cycles (normally 6–7% decrease), while detectable, are not large enough to influence our conclusions. In addition, unlike tissue samples from an adult animal, FPMs are still slowly remodeling on the second day after their formation. Repetitive stretch cycles could modulate the remodeling process and so introduce an additional variable into the experiment that could be difficult to control. Effects of stretching on the tissue remodeling process will be the subject of future investigation. Prestretching also reduces the variability of force versus stretch properties from one FPM to another. In the following we use the second and third stretch cycles for our experimental measurements. Similar behavior is seen for biological tissues, although many rather than only one preconditioning stretches are used to reach a state in which force versus strain curves are repeatable (Fung, 1993). Furthermore, the variation of force with strain is quite similar when the strain rate is doubled. Although the loading and unloading curves differ, each is repeatable and relatively insensitive to strain rate over this narrow range of slow strains (Fung, 1993).

Uniformity of strain

During first (preconditioning) stretch local strain is inhomogeneous, and in some regions irreversible. During later stretches the strain appears homogeneous and reversible throughout the tissue. The local strain was measured by following the displacement of small markers embedded throughout the FPM. Time-lapse images of the sample were taken every 2 min of each stretch cycle in the same apparatus described above (Fig. 1) using a video camera with a magnifying lens focused on the sample through the transparent organ bath. The displacements of markers made from small pieces of sterilized silk surgical suture ($<$0.5 mm in length) were traced using Scion-image software (PC version of NIH-image). During the first stretch the local strain in the portions of the tissue closest to the horizontal bars around which the FPM was looped were larger than the in the middle of the tissue. Moreover, the markers in the regions closest to the bars did not return to their original positions after the first stretch. In the second and subsequent stretches the local strain measured by the markers appeared uniform and reversible in all parts of the FPM.

Structural components that resist strain

The force versus strain curve for a prestretched FPM activated to nearly the maximum extent by 20% FCS is shown in Fig. 4 *a* as the curve labeled "Total." After acquisition of this curve, the FPM was treated with 2 μM CD, which disrupts the actin cytoskeleton, and was stretched again to obtain the curve labeled "Passive." The difference between the total and the passive curves is labeled "Active." The force versus strain curves exhibit hysteresis: force is larger during tissue loading than during unloading. Fig. 4 *a* illustrates that the elastic properties of the passive and active components are different: the active component of force increases approximately linearly with strain, the passive component increases approximately exponentially. Qualitatively similar behavior is seen in Fig. 4 *b* for the active and passive components of dynamic stiffness (measured at 0.5 Hz). Similar results were obtained when active and passive components were both determined from second stretches of different FPMs, hence the small decrease in peak force between second and third stretches (Fig. 3) has no significant effect on these results.

Disruption of the intermediate filament and microtubule cytoskeletal systems does not cause a substantial change in the mechanical properties of FPMs beyond that caused by CD. This is demonstrated by treating FPMs with the phosphatase inhibitor, calyculin A, at high concentration, which has been reported to disrupt actin, microtubule, and vimentin cytoskeletal networks (Chartier et al., 1991; Eriksson et al., 1992; Hirano et al., 1992). The force-strain and stiffness-strain curves of FPMs treated with calyculin A are not significantly different from those of FPMs treated with CD (Fig. 5). Using CD, therefore, we can decompose the stiffness of FPMs into two additive components: the passive component from which the cytoskeletal contributions of the cells (and possibly some portion of the ECM) have been eliminated, and the cytoskeleton-dependent active component.

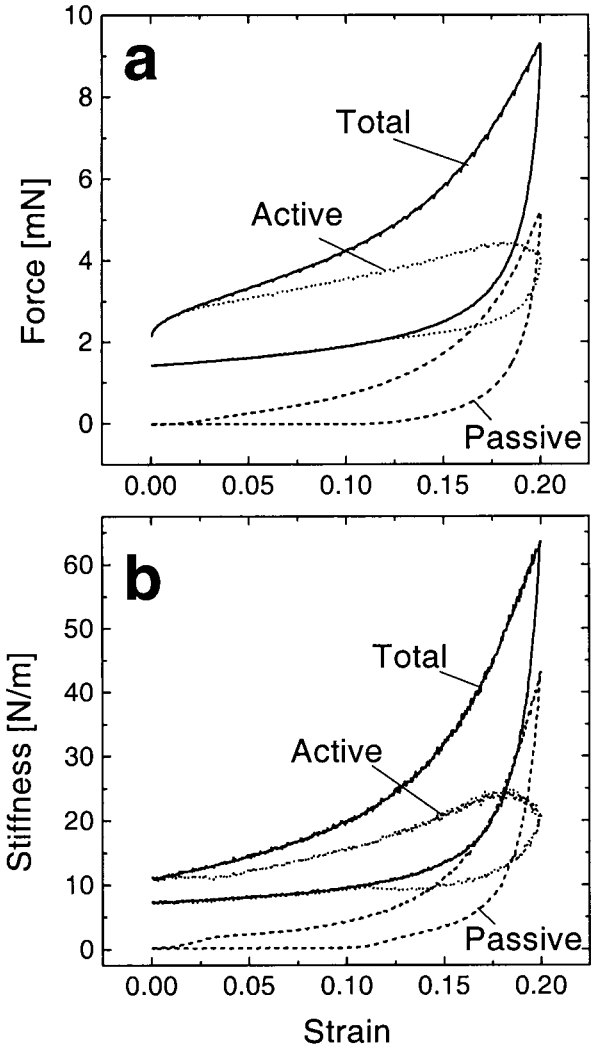

FIGURE 4 Force and stiffness versus strain for activated and CD-treated FPMs. The force versus strain (*a*) and dynamic stiffness versus strain (*b*) for a prestretched FPM activated by 20% CS is shown by solid lines labeled "Total." The force and stiffness curves obtained after treatment by 2 μM CD are shown by broken lines labeled "Passive." The difference between the Total and the Passive curves, labeled "Active," is shown by dotted lines. All the curves exhibit hysteresis. The Active curves increases approximately linearly with strain; the Passive curves increases approximately exponentially. The dynamic stiffness was measured at 0.5 Hz (*b*).

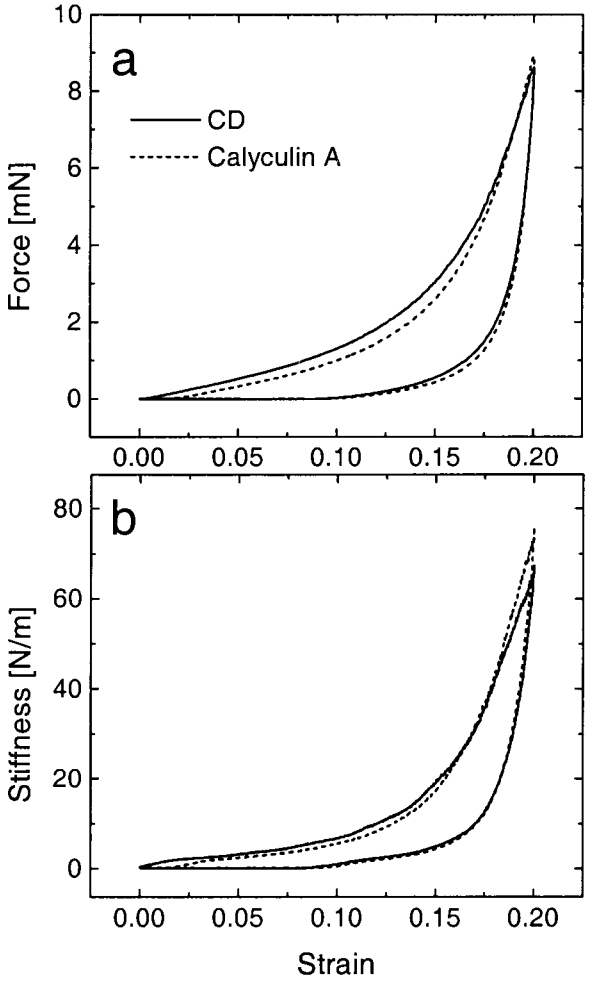

FIGURE 5 Effects of calyculin A and CD on FPMs. Two duplicate FPMs were subjected to a preconditioning stretch, treated with 20% CS, and then stretched a second time to characterize the activated FPMs. One FPM was then treated with the phosphatase inhibitor calyculin A (10 nM), known to disrupt actin, microtubule, and vimentin cytoskeletal networks (*broken lines*). The other sample was treated with 2 μM cytochalasin D (*solid lines*). The force-strain (*a*) and stiffness-strain (*b*) curves of the FPM treated with calyculin A are not significantly different from those of the FPM treated with CD. This indicates that no significant contribution to the mechanical properties measured in the dynamic range used in this work (strain rate of 1.6 μm/s up to 20% strain plus 40 μm amplitude sinusoidal oscillation at 0.5 Hz) are detected from the cytoskeletal filament systems other than the actin system. (Note that mechanical effects of intermediate filaments and microtubules that required an intact actin cytoskeleton would not be detected by this measurement.)

The magnitude of the active force increasing linearly with strain remains greater up to ~20% strain than that of the passive component that increases exponentially. It is also noteworthy that the active force level diminishes with increasing strain at strains >~17% (Fig. 4 *a*). In muscle, this behavior is thought to result from a decrease in the overlap between actin and myosin filaments (Murphy, 1980). To determine whether a similar mechanism is involved in FPMs would require correlation of force with a parameter analogous to sarcomere spacing in a skeletal or cardiac muscle. This would be difficult to accomplish in the fibroblasts in an FPM.

Analogous results are obtained in measurements on FPMs, which have not been activated by FCS (data not shown). In contrast to relaxed muscle, nonactivated FPMs exert a basal level of contractile force, which persists even after the first conditioning stretch. Hence, under the conditions of these experiments, the nonactivated FPM retains some actin-myosin interaction. Measurements of the phosphorylation of the regulatory light chain of nonmuscle my-

osin demonstrate that myosin is partly activated under these conditions (cf. Kolodney and Elson, 1993).

Although the active cellular contribution to the "total" force versus strain curve is largely eliminated by CD, the effect of the matrix compression and remodeling by the cells is large and persists after CD treatment. Fig. 6 illustrates that even after treatment by 2 μM CD, the FPM is much stiffer than a collagen matrix gelled without cells. This difference in mechanical properties results from the remodeling of the matrix by the cells during the period in which the matrix is compressed. A residual cross-linking of matrix filaments by the cells could persist after CD treatment.

The active curve was obtained by subtracting data obtained during a third stretch from data obtained in a second stretch. To assess the influence of the small reduction in maximum force between second and third stretches, an active curve was obtained from two second stretches on different FPMs, one treated with CS, the other with both CS and CD. The active curve obtained in this way from duplicate samples had ~6% smaller maximum force than the curve obtained using second and third stretches on the same FPM. The shapes of the curves obtained using the two different methods were qualitatively indistinguishable, hence active and passive mechanical parameters measured using sequential stretches might be overestimated and underestimated, respectively, by ~6%.

Dependence of dynamic stiffness on the oscillation frequency of force and strain

A plot of the dynamic stiffness of an activated FPM measured at 0.5 Hz over the range of strains from 0 to 20% is shown in Fig. 4 *b*. Unlike a linear elastic spring with stiffness independent of strain, the dynamic stiffness of the FPM increases with increasing strain. The plots of stiffness versus strain for the total, active, and passive components are qualitatively similar to the plots of force versus strain for the same components. Replotting these data reveals a striking linear dependence of stiffness on stretching force (Fig. 7). Similarly, stiffness also shows a linear variation with contractile force generated by the cells in the FPM. Fig. 8 shows that stiffness increases in parallel with force after activation by serum and decreases in parallel with force after treatment by CD. The proportionality constant for the dependence on stretching force, ~0.008 μm^{-1}, is similar to that for the cell-generated force, 0.005 μm^{-1}, even though

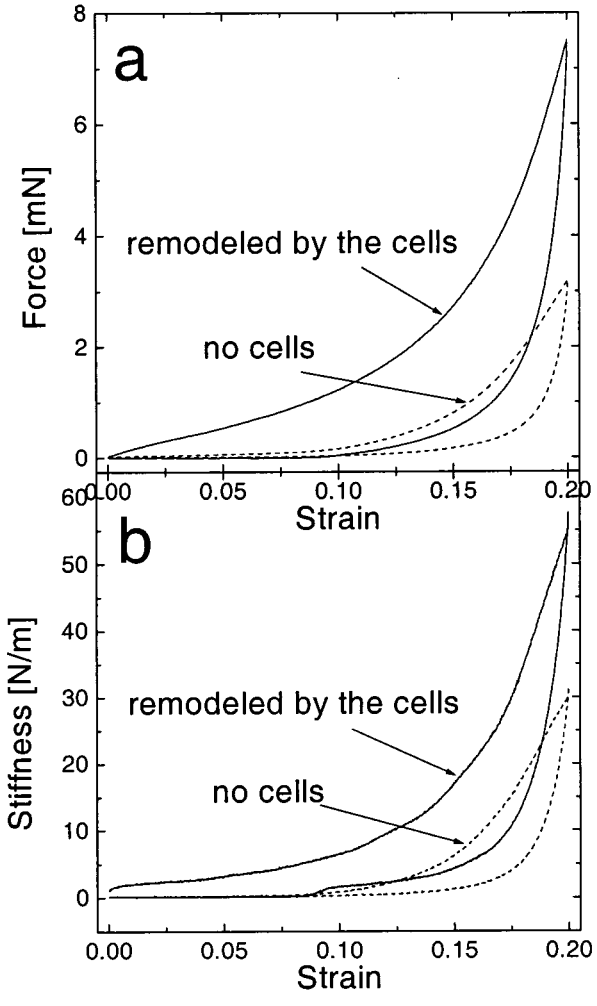

FIGURE 6 The effect of cells on the mechanical properties of the matrix. The force-strain (*a*) and stiffness-strain (*b*) relationships for a collagen matrix remodeled by fibroblasts for 2 days after casting and then treated with CD to eliminate cytoskeletal contributions to the mechanical properties (*solid curves*) and for a collagen matrix prepared similarly but without cells (*broken curves*).

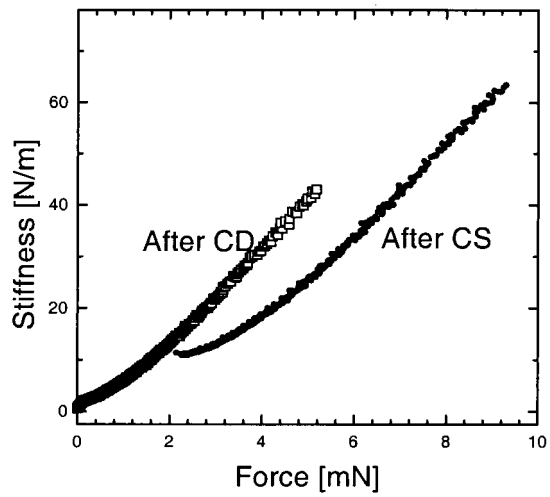

FIGURE 7 Stiffness versus imposed force. Replotting the force-strain and stiffness-strain relationships in terms of stiffness versus force reveals a striking linear dependence of stiffness on the stretching force. These data were obtained from the loading (stretching) curves for serum-activated (*filled circles*) and CD-treated (*open squares*) FPMs.

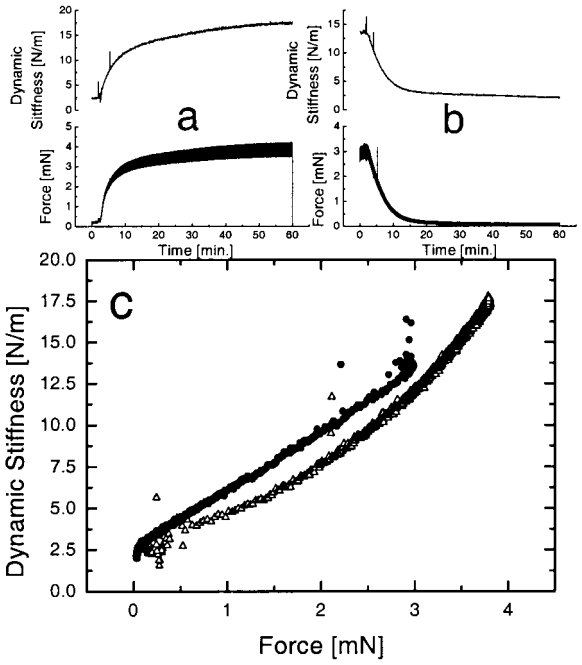

FIGURE 8 Stiffness versus cell-generated force. Stiffness versus force relationships for FPMs for which the force changes resulted from activation by serum (*a*) and from treatment by CD (*b*) under isometric conditions. The stiffness is a remarkably linear function of the isometric force induced by these treatments (*c*).

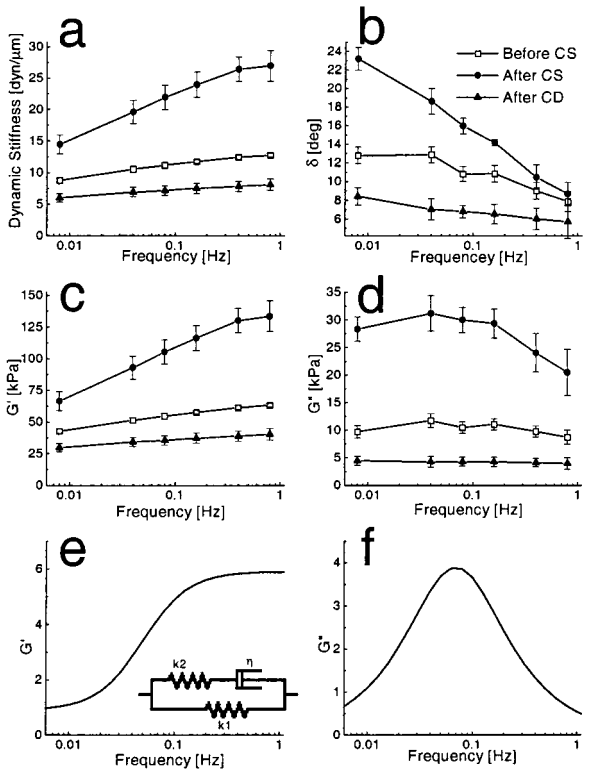

FIGURE 9 Dynamic stiffness, phase delay, storage, and loss modulus as functions of frequency. For activated (*filled circles*), unactivated (*open squares*), and CD-treated (*filled triangles*) FPMs the dynamic stiffness increases almost linearly with $\log(\nu)$ (*a*) and the phase angle decreases with increasing frequency from 0.008 to 0.4 Hz (*b*). The values of both the phase delay and the dynamic stiffness are largest and depend most sensitively on frequency for the activated FPMs. Storage and loss moduli, G' and G'', respectively, were calculated from the dynamic stiffness and phase angle. The G' increases with $\log(\nu)$ similarly to the dynamic stiffness (*c*). The G'' showed a maximum at around 0.04 Hz, especially for the activated FPMs (*d*). The G' and G'' are simulated using the standard linear solid model shown in panel *e*. Using appropriate constants for k_1, k_2, and η, the G' increases with $\log(\nu)$ (*e*) and the G'' shows a maximum at a similar frequency to the experiment (*f*). The points are averages of 4 samples and the bars represent standard deviations.

the measurements were performed on FPMs prepared on different occasions.

As expected for a viscoelastic system, the dynamic stiffness varies also with the rate of stretch (oscillation frequency). Fig. 9 *a* demonstrates that the dynamic stiffness increases almost linearly with $\log(\nu)$ from 0.008 to 0.4 Hz for activated, inactivated, and CD-treated FPMs. We have obtained data up to 10 Hz, which showed a similar trend, but due to limitations of the measurement system, these data are less reliable than the measurements up to $\nu \sim 2$ Hz. As before, higher stiffness values are associated with higher values of force. Also, the rate at which stiffness increases with $\log(\nu)$ is greater the larger the stiffness. These measurements were carried out on prestretched FPMs that had been returned to zero initial strain to emphasize the cellular contribution to the dynamic stiffness. Under these conditions the stiffness of the CD-treated FPM is low and increases little with increasing ν (Fig. 9 *a*). The dynamic stiffness results mainly from the active component, which dominates mechanical properties of the FPM at low strain.

The storage and loss moduli, $G'(\nu)$ and $G''(\nu)$, respectively, indicate the portions of the energy required to deform the FPM that are either stored or dissipated as heat. In a sinusoidal deformation occurring at frequency ν, $G'(\nu)$ is the force in phase with the strain and $G''(\nu)$, the force 90° out of phase with the strain, both divided by the strain (Ferry, 1980). G' and G'' are plotted for non-activated, activated, and CD-treated FPMs in Fig. 9, *c* and *d*. Both G' and G'' markedly increase after activation by CS, but for all conditions G' is substantially greater than G''. Hence, for these FPMs the elastic resistance to stretching substantially exceeds viscous resistance. The G'' of the activated FPMs showed a maximum at ~0.4 Hz, and the maximum disappeared by CD treatment. It suggests the actin-myosin interaction contributes largely to viscosity of the FPMs. The experimental results are compared to a simple linear standard solid model (Fig. 9, *e* and *f*). For appropriate values of the springs, k_1 and k_2, and the dashpot viscosity, η, we see that the increase of G' over the frequency range of the measurements and the maximum observed for G'' are both qualitatively reproduced. Nevertheless, it is clear that for the FPMs the frequency range over which G' increases and the

breadth of the maximum of G'' are significantly greater than observed for the simple model, which is characterized by a single relaxation process. This suggests that for the tissue models a spectrum of relaxation times contributes to the mechanics, as has been observed for natural biological tissues (Fung, 1993).

Another indicator of the dependence of the mechanical properties on rate of stretch is the phase delay, δ, between the sinusoidal driving function and the force response. This phase delay depends on the viscosity of the material and is related to the storage and loss moduli as $G''/G' = \tan \delta$. The viscous damping energy is calculated as follows. The time-dependent applied strain, $\epsilon(t)$, is defined as $\epsilon(t) = \epsilon_0 \sin \nu t$. The stress, $\sigma(t)$, i.e., the force per unit cross-sectional area, A, of the sample, is defined as, $\sigma(t) = F(t)/A = \sigma_0 \sin(\nu t + \delta)$. The energy loss per cycle of the oscillation per unit volume of tissue, ΔW, is the integral of the work done in one cycle, T, which is

$$\Delta W = \int_0^T \sigma(t) \frac{d\epsilon(t)}{dt} dt = \pi \sigma_0 \epsilon_0 \sin \delta.$$

The fractional damping energy is calculated by normalizing ΔW by the maximum energy, W, that the system could store elastically for a given strain amplitude. The quantity W is obtained by integrating the work done in a quarter cycle without phase delay, which is

$$W = \int_0^{T/4} \sigma(t) \frac{d\epsilon(t)}{dt} dt = \frac{\sigma_0 \epsilon_0}{2}.$$

Therefore, the normalized damping energy, $\Delta W/W$, is equal to $2\pi \sin \delta$, which is independent of the strain and stress amplitude and depends only on the phase angle (Findley et al., 1976). Hence, we have used δ as an indicator of the viscosity of the FPMs. The values of δ for FPMs before and after activation and after treatment with CD are shown in Fig. 9 *b*. The value of δ decreases with increasing frequency and more rapidly, the higher the stiffness. If we further decreased the oscillation frequency, the value of tan δ might start to decrease, as is seen in the standard linear solid viscoelastic model. There should be a lower limit to the frequency dependence of the mechanical response that is due to the material properties of the FPM. The slow active responses of the living cells within the matrix can, however, also modulate the properties of the FPM at low frequencies.

Dependence of mechanical properties on cell concentration

The active force and stiffness of an FPM depends on the number of cells it contains. This is demonstrated by comparing the mechanical properties of FPMs assembled with initial cell concentrations of 1.0, 0.7, 0.4, and 0.1×10^6 cells/ml (Fig. 2). As illustrated in Fig. 10, the active force and stiffness vary roughly in proportion to the initial number of cells in the range $0.4–1.0 \times 10^6$ cells/ml. In contrast, the force and stiffness for the passive component is independent of input cell number over this range. The FPM initiated with 0.1×10^6 cells/ml has disproportionately low force and stiffness in comparison to the model tissues with higher numbers of cells (see below).

Stress and elastic modulus

The mechanical characteristics of the model tissues are more readily interpreted when expressed in terms of stress (force/unit cross-sectional area of tissue) and elastic modulus (stiffness $\times$ length/unit cross-sectional area of tissue). These material properties should be independent of the shape and size of the model tissues and so can be more readily compared from one tissue to another. In this comparison we assume that differences in stress and stiffness are due to differences in material properties rather than to differences in tissue microarchitecture; we effectively assume that our test specimens are homogeneous and isotropic. If there are systematic variations in the density and orientations of the cells, this must be taken into account using a more detailed analytical approach. The first step in the development of a theoretical model that accounts for FPM mechanics in terms of the organization and properties

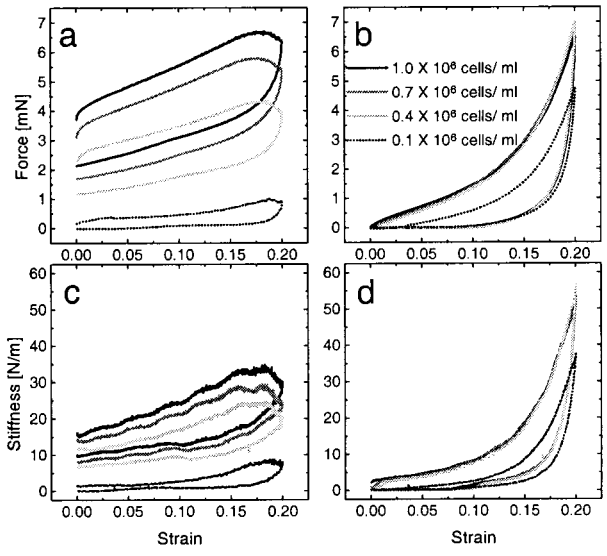

FIGURE 10 Dependence of force and stiffness on cell number. The force-strain (*a*, *b*) and stiffness-strain (*c*, *d*) curves for the active and passive components of FPMs assembled with initial cell concentrations of 1.0, 0.7, 0.4, and 0.1×10^6 cells/ml are shown by black solid, gray solid, light gray solid, and dotted lines, respectively. The active force (*a*) and stiffness (*c*) vary roughly in proportion to the initial number of cells. In contrast, the force (*b*) and stiffness (*d*) for the passive component are independent of input cell number. The FPM initiated with 0.1×10^6 cells/ml has a disproportionately low force and stiffness.

of the constituent cells and matrix is presented by Zahalak et al. (2000). The cross-sectional areas of the FPMs were measured as described under Methods. As shown in Fig. 11, the thickness of the FPMs decreases with increasing numbers of cells, although the extent of compression appears to be approaching a limit at the highest cell concentration. Stress and elastic modulus at zero strain were computed by dividing the force and stiffness by the cross-sectional area of the unstrained FPMs. Then stress and modulus were calculated at higher strains by assuming incompressibility of the tissue to calculate the variation of cross-sectional area with strain (Fig. 12). As do the force and stiffness, the stress and elastic modulus of the active component increase as the initial concentration of the cells increases. In contrast to the force and stiffness, however, the stress and elastic modulus of the passive component also increased with increasing initial concentration of cells. Normalization of the force and stiffness with respect to the total cross-sectional area of the tissue yields intensive mechanical properties. It is still more informative, however, to normalize the active force with respect to the cross-sectional area of the cells and the passive component with respect to the cross-sectional area of the matrix.

The fraction of the cross-sectional area of an FPM occupied by cells is determined from confocal images of FPMs in which the cells were loaded with a cytoplasmic fluorophore, as explained above. The stack of confocal images, acquired with the image planes parallel to the long axis of the tissue, were computationally resliced to provide a sequence of optical sections perpendicular to the long axis of the tissue (Satoh et al., 1996). Using a threshold as described under Methods, the fluorescent cytoplasmic volume was discriminated from the ECM and integrated within the image planes to provide the ratio of cytoplasmic to total FPM area. The ratios of the cross-sectional area of the cells divided by that of the FPM are plotted versus distance along the tissue axis for different initial cell concentrations in Fig. 13 *a*. The averaged ratio is linearly related to the number of cells initially incorporated into the model tissues (Fig. 13 *b*). Fibroblasts embedded in collagen gels have been shown to slow their proliferation significantly (Schor, 1980). Inasmuch as our samples were cultured only for 2 days before the experiment, including 16 h of serum starvation, the increase in cell number is expected to be minimal. It is noteworthy that only in the samples with an initial cell concentration of 0.1×10^6 cells/ml does the average cell density in the images approach zero at various locations along the axis of the tissue.

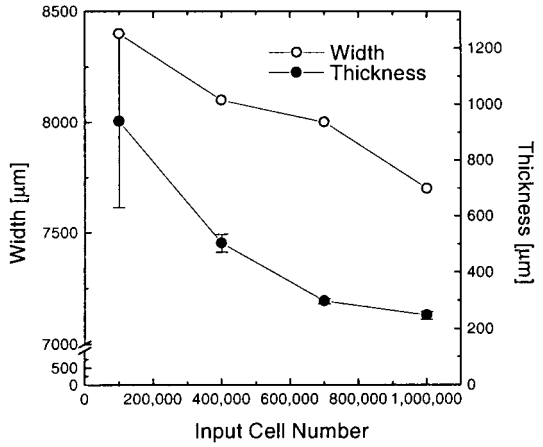

FIGURE 11 Dependence of FPM thickness on cell number. Thickness and width were measured on FPMs that had been compressed by the cells during two days of matrix remodeling after gelation of the collagen. The thickness and width of the FPMs decrease with increasing numbers of cells, although the extent of compression appears to be approaching a limit at the highest cell concentration.

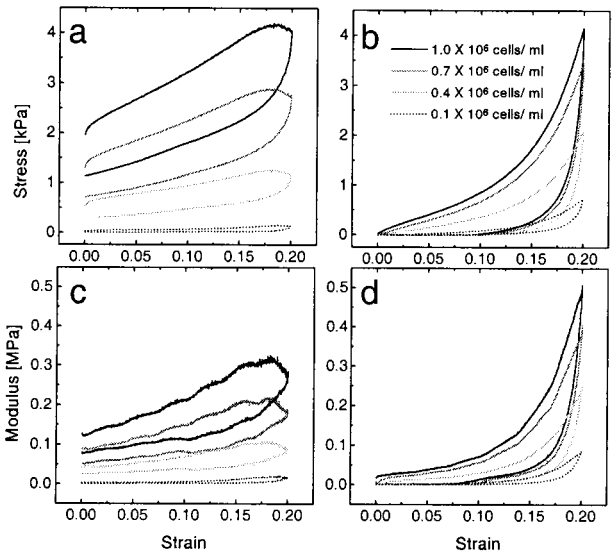

FIGURE 12 Stress and modulus relative to entire cross-sectional areas of FPMs. Stress and elastic modulus (Cauchy stress and modulus, see text for details) obtained by dividing the force and stiffness by the entire cross-sectional area of the FPMs assembled with initial cell concentrations of 1.0, 0.7, 0.4, and 0.1×10^6 cells/ml are shown by black solid, gray solid, light gray solid, and dotted lines, respectively. The stress and elastic modulus of both the active component (*a*, *c*) and of the passive component (*b*, *d*) increase as the initial concentration of the cells increases.

The mean value of the cross-sectional area of the FPM was used to compute the active stress, σ_A, elastic modulus, E_A, passive stress, σ_P, and elastic modulus, E_P. The active stresses were computed by normalizing the active and passive forces, F_A and F_P, by the cross-sectional area of the FPM, A. Then $\sigma_A = F_A/A$ and $\sigma_p = F_P/A$. To compare with measurements on single cells (Tables 2 and 3) it is also informative to compute the active stress and modulus, σ_a and E_a, and the passive stress and modulus, σ_p, and E_p, normalized by the total cross-sectional areas of the cells and matrix, A_A and A_P, respectively. The total cross-sectional area of the FPM is $A = A_A + A_P$ (Fig. 13). Then $\sigma_a =$

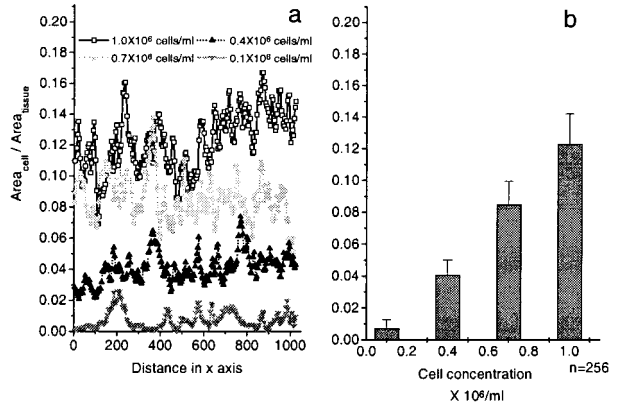

FIGURE 13 Fraction of FPM cross-sectional areas occupied by cells. The fraction of the cross-sectional area of a FPM occupied by cells was determined from confocal images of FPMs. The fractional cell area of FPMs assembled with initial cell concentrations of 1.0, 0.7, 0.4, and 0.1 $\times$ 10^6 cells/ml are plotted against the position along the tissue axis (east and west direction on the image plane) by open squares, light gray filled squares, filled triangles, and filled gray down-triangles, respectively (*a*). It is noteworthy that only in the samples with an initial cell concentration of 0.1 $\times$ 10^6 cells/ml does the average cell density in the images reach zero at various locations along the axis of the tissue. The averaged fractional cell areas increase almost proportionally to the initial cell concentration (*b*).

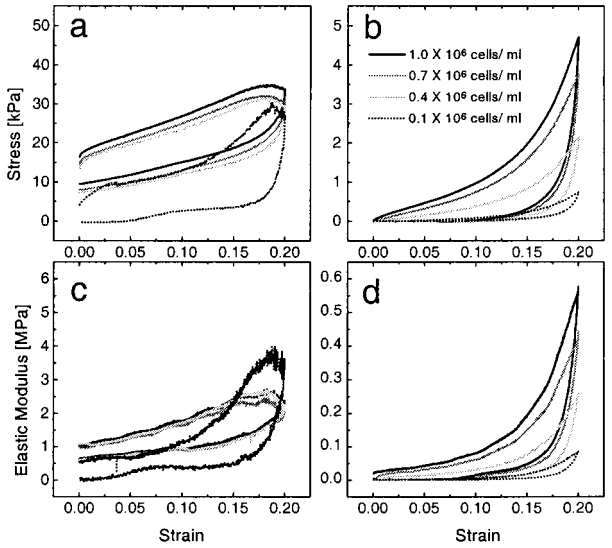

FIGURE 14 Specific stress and modulus relative to cross-sectional areas of cells and matrix. Active stress and elastic modulus were obtained by dividing the active force and stiffness by the total cross-sectional area of the cells. Passive stress and elastic modulus were obtained by dividing the passive force and stiffness by the total cross-sectional area of the FPM minus the area of the cells. Black solid, gray solid, light gray solid, and dotted lines represent data computed from FPMs assembled with initial cell concentrations of 1.0, 0.7, 0.4, and 0.1 $\times$ 10^6 cells/ml, respectively. The active stress and elastic modulus are very similar for each FPM except the one with the lowest cell number (*a*, *c*). In contrast, the passive component shows a stronger dependence on cell concentrations (*b*, *d*):

$F_A/A_A = \sigma_A/R_c$ and $\sigma_p = F_P/A_p = \sigma_P/(1 - R_c)$, where $R_c = A_A/A$. (Note that $\sigma_A + \sigma_p = \sigma_T$, the modulus for the entire tissue model. In contrast, $\sigma_T \neq \sigma_a + \sigma_p$.). The elastic moduli were computed by using the same principles.

The curves representing active mechanical properties (stress and elastic modulus) became very similar to each other when expressed in terms of the cross-sectional area of the cells, except for the tissue with the lowest cell number (Fig. 14). Hence, for the FPMs with the three higher cell concentrations, the force exerted per cell estimated using the normalization method was the same in each tissue independent of initial cell concentration. This result strongly supports the concept that the "active" component represents a specific contribution of the cells to the mechanical characteristics of the tissue. In contrast, the passive component normalized with respect to the area of the ECM showed a stronger dependence of mechanical parameters on the cell concentrations: the higher the cell concentration, the higher the stress and elastic modulus. This suggests that the extent of stiffening by collagen remodeling increases with the cell concentration (cf. Figs. 12 and 14).

The active mechanical properties estimated from the data obtained at the lowest cell concentration are significantly different from those at the other concentrations. This indicates a failure of the assumption of similarity of the distributions of the cells in the FPMs. As seen in Fig. 13, the FPM with the lowest concentration of cells shows some cross-sections that contain no cells. For FPMs with higher initial cell concentrations all cross-sections contained cells. Hence, at the lowest cell concentrations, fluctuations in cell number along the axis of the FPM were relatively large. This correlates with the exceptional values of stress and modulus for the FPM with the lowest cell concentration in contrast to the similar stress and modulus seen in FPMs with higher concentrations and more homogeneous distributions of cells (Fig. 14). Perhaps more important is the possibility that the cells at the higher concentrations could approach the formation of a separate continuous phase embedded within the ECM. In contrast, at the lowest concentration, the sections in which no cells were present represent discontinuities in the cellular phase (Fig. 13).

The magnitudes of the stress and modulus of the cells are much higher than those of the ECM (Fig. 14). We expect that at longer incubation times the ECM and the tissue overall would become much stiffer due to further compression of the matrix, de novo ECM synthesis, or the enzymatic cross-linking of ECM filaments (Huang et al., 1993).

DISCUSSION

Mechanical measurements on FPMs

We describe a simple, flexible approach for measuring the mechanical characteristics of reconstituted model tissues (Fig. 1). In the FPMs studied in this work the cells have compressed the matrix to ~10% of its original volume

while also stiffening the tissue and establishing a "basal" contractile force. This remodeling is probably similar to processes that occur in normal tissue development and wound healing. Its mechanism has been studied but is not yet fully understood (Grinnell, 1994; Stopak and Harris, 1982). The FPMs that we have studied have undergone a phase of compression, stiffening, and force development over 1–2 days in culture, but further slower mechanical changes continue over extended time periods due to cellular reorientation and additional matrix cross-linking (Huang et al., 1993). The matrix components of the FPMs are initially in a mechanically metastable state. They are reduced by a single preconditioning stretch cycle to a state with somewhat lower stiffness in which repeatable force and stiffness versus strain curves can be obtained. FPMs developed under different culture conditions, e.g., with different amounts of serum present, or assembled with cells other than CEF, differ with respect to the extent and time course of matrix compression, stiffening, and basal force. Characterization of the mechanics of FPMs at both earlier and later stages of development than those studied for this work will be deferred to a later time. Some aspects of the early stages of development of fibroblast-containing model tissues have previously been studied (Barocas et al., 1995; Eastwood et al., 1996).

Distinguishable contributions of cytoskeleton and matrix

As a preconditioned FPM (activated with 20% calf serum) is slowly stretched, the force increases nonlinearly with the strain. As the strain is reduced, the force drops rapidly so that there is a substantial hysteresis between the loading and unloading curves (Fig. 4 *a*). These curves are repeatable and relatively independent of small changes in rate of strain. As discussed below, however, the dynamic stiffness does increase significantly with strain rate at higher strain rates, indicating significant time-dependent mechanical behavior.

When the FPM is treated with CD to disrupt the actin cytoskeletons, the force over the entire range of strains from 0 to 20% is reduced (Fig. 4 *a*). For strains between 0 and 2.5% these forces, measured in both loading and unloading, are negligible compared to the values measured for the untreated FPM. A simple, provisional phenomenological model (Fig. 15) provides a structural vantage from which to interpret the results. We suppose that the cellular contributions are dominated by the actin cytoskeleton. This includes a contractile component (CC) dependent on actin-myosin interactions and a series cellular (SC) component, which includes the substantial portion of the actin cytoskeleton that does not directly interact with myosin. Cells connect to the extracellular matrix via structures that bind to the cortical actin filaments (Luna and Hitt, 1992). Therefore, we have also included a series matrix (SM) component, which depends on the integrity of the actin cytoskeleton. Ex hypothesis, CD completely eliminates the CC and SC (and, therefore, the SM) components. We have also included a parallel cellular (non-actin) component, PC, to account for possible residual cellular contributions to the mechanics of CD-treated FPMs. The contributions of the matrix parallel to the cells is represented by PM, which we assume is not directly affected by CD. The passive component is represented by PC + PM, the active component by SC, CC, and SM. In this model we assume that the variation of force with strain for PM and PC is independent of that for SC + CC + SM and that the contributions of the three parallel branches in Fig. 15 can be simply added to yield the behavior of the intact tissue. For purposes of illustration, suppose that each of the elements in the model behaves as a simple elastic spring. Then it is straightforward to show that the spring constant for the tissue overall is $k = k_{pm} + k_{pc} + (1/k_{sm} + 1/k_{sc} + 1/k_{cc})^{-1}$, where k_{pm}, k_{pc}, k_{sm}, k_{sc}, and k_{cc} are the spring constants for the parallel matrix, parallel cell, series matrix, series cell, and contractile elements. The effective spring constant or stiffness for the passive component is $k_{pm} + k_{pc}$; that for the active component is $(1/k_{sm} + 1/k_{sc} + 1/k_{cc})^{-1}$. If SM is very stiff ($k_{sm} \to \infty$), then the stiffness of the active component $(1/k_{sc} + 1/k_{cc})^{-1}$ is determined only by cellular constituents. In general, however, the relative magnitudes of k_{sm}, k_{sc}, and k_{cc} are unknown, and so we must regard the stiffness of the active component as including a contribution from that portion of the extracellular matrix that is connected to the actin cytoskeleton. Similarly, if $k_{pm} \gg k_{pc}$, then the stiffness of the passive component depends only on the state of the ECM. In general, however, we must acknowledge that there could be cellular contributions to the behavior of the matrix, especially in cross-linking matrix filaments via cellular structures. An important task for the future is to estimate the relative magnitudes of the various spring constants in this model to provide an assessment of the mechanical contributions of the structural elements in the model.

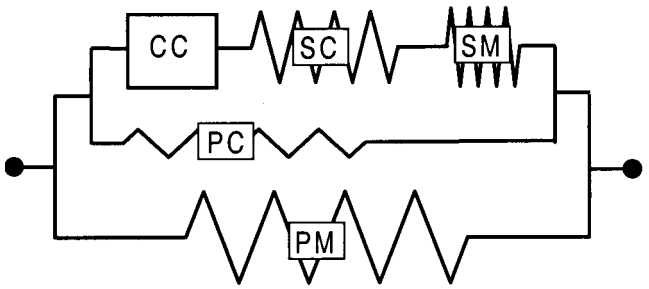

FIGURE 15 Schematic model of FPM mechanics. In this schematic model the contractile (CC), the series cytoskeletal (SC), and the series matrix components (SM), all in series, are mechanically connected in parallel with the parallel cellular component (PC) and the parallel matrix component (PM). CD treatment eliminates CC and SC (and therefore SM), from the total tissue mechanics.

There could be noncytoskeletal cellular contributions to the passive component. Treatment of nonactivated FPMs with the nonionic detergent Triton X-100 (0.2% in 150 mM NaCl) caused up to a 30% reduction of force below the level observed with CD treatment (result not shown). Under these high salt conditions detergent extraction disrupts not only cellular membranes, but also the cytoskeleton. Hence, this experiment suggests the extent to which nonmembranous, noncytoskeletal cellular structures might contribute to the passive mechanical properties of FPMs. These effects might arise from cellular cross-linking of matrix strands or from the space-occupying properties of the nucleus. Interpretation of these experiments is complicated, however, by uncertainty about the effect of the detergent on the structure of the matrix independent of its effects on cell membranes.

We have tested the proposition that active forces generated by the cells are approximately independent of matrix forces caused by stretching by determining the increment of force resulting from serum stimulation when the FPM has been strained to different extents. As seen in Fig. 16, the force increment is roughly independent of the strain level even though the stresses sustained by PC + PM are different at different strains. If we suppose that the same contractile force is generated by the cells in response to serum at each level of strain, this experiment indicates that the forces exerted or sustained by the cellular compartment of the tissue are measured independently of the stresses sustained by the matrix component.

A similar conclusion is suggested by the observation that at a specified strain, the average stress on the cellular compartment of the tissue model is independent of initial cell concentration, even though the stress sustained by the PC + PM at each strain varies with cell concentration (Fig. 14). Hence, variations in the mechanical contributions of PC + PM do not strongly influence measurements of force exerted by the active component.

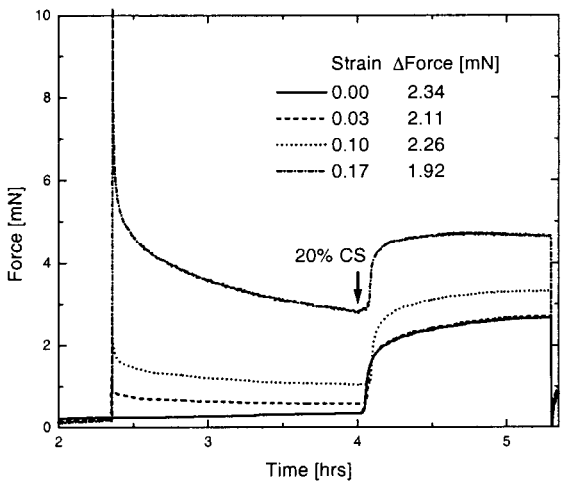

FIGURE 16 Dependence of active force on strain. Identically prepared FPMs were subjected to strains of 0.00, 0,03, 0.10, and 0.17 (shown as *solid*, *broken*, *dotted*, and *broken dot lines*, respectively). After the force reached a steady level at each strain, 20% CS was added and the increase in force due to myosin activation was recorded. The force increments are roughly independent of the initial strain level.

Even after the disruption of the actin cytoskeleton, vimentin intermediate filaments, microtubules, or other cellular structures might provide a cellular contribution to the parallel cellular component (PC) that remains after CD treatment. We have assessed this possibility by using the phosphatase inhibitor calyculin A. Treatment of cells with a high concentration of calyculin A disrupts intermediate filaments and microtubules as well as actin filaments (Hirano et al., 1992). We have verified this effect on intermediate filaments and microtubules in FPMs (data not shown). Fig. 5 demonstrates that force and stiffness during a slow stretch experiment, measured in FPMs in which intermediate filaments and microtubules are disrupted, are not significantly different from the corresponding measurements in which the actin cytoskeleton has been disrupted by CD. This suggests that the cytoskeletal contribution to PC is negligible, although it is still possible that microtubules and intermediate filaments exert some effect on mechanics via the actin cytoskeleton. These effects could not be observed in CD-treated cells. Preliminary observations of FPMs containing cells lacking functional vimentin intermediate filaments, however, indicate that these filaments contribute little to the mechanical properties of FPMs with intact actin cytoskeletons at the strain levels used in these experiments (Wakatsuki, Elson, and Wysolmerski, unpublished results). Because the mechanical properties of a cell are dominated by its cytoskeleton (Petersen et al., 1982), it seems unlikely that PC exerts a significant effect on FPM mechanics except, possibly, via cellular cross-linking of matrix filaments. Even this effect, however, is expected to be small. The cell is linked to the ECM through matrix attachment sites provided by integrins or the dystrophin system via actin filaments (Luna and Hitt, 1992), and so should be vulnerable to disruption by CD. There could also be some influence of the space-occupying properties of the nucleus on the FPM mechanics.

In sum, we have *operationally* defined additive active and passive contributions to the mechanics of FPMs. CD eliminates the active contributions; the passive contributions remain after CD treatment. The active cellular component is dominated by cytoskeletal structures (CC and SC) but there can also be an active matrix component arising from ECM structures that interact directly in series with the actin cytoskeleton (SM). For example, microfilament bundles are linked to the ECM through focal adhesions. Hence, disruption of actin filaments by CD could influence the mechanical properties of the matrix. The passive component is dominated by the ECM (PM) but is also potentially influenced by passive cellular structures that survive CD-treatment (PC). We expect that a cytoskeletal perturbation would largely appear as an effect on the active component,

while a change in ECM structure would mainly influence the passive component.

The active component

Fig. 14 demonstrates that the dependence on strain of the force and stiffness of the active component changes apparently discontinuously when the density of the cells is reduced below a critical level. This suggests that the cells form a structurally coherent substructure within the FPM when the initial cell density is equal to or greater than 400,000 cells/ml. When the initial density is reduced to 100,000, however, the cells are apparently too sparse to form this network. This hypothesis is supported by the observation that there are cells present in all cross-sections observed for tissue models with initial cell densities of 400,000 and above, but that sections devoid of cells are seen for tissue models with initial densities of 100,000 cells (Fig. 13). This structural coherence of the cellular compartment could arise either if there were sufficiently strong direct mechanical connections among the cells or if the ECM elements linking the cells (the SM component in Fig. 15) were sufficiently stiff.

That calyculin A causes no additional reduction of force or stiffness relative to CD indicates that contributions of the cells are dominated by the actin cytoskeleton at the strains used in these experiments (Fig. 5). This result is consistent with results from cell indentation measurements (Petersen et al., 1982) and also with expectations from rheological measurements of the purified actin microfilaments, microtubules, and vimentin intermediate filaments (Janmey et al., 1991). (As pointed out above, however, it is still possible that microtubules and intermediate filaments could make a substantial mechanical contribution if that contribution were dependent on the integrity of, i.e., were mechanically in series with, the actin filament system.)

It is difficult to directly test the specific cellular contributions to the FPMs because the mechanical characteristics of the cellular components cannot be measured in the absence of the ECM. The matrix is essential to the integrity of the FPM, and so the state of the matrix could influence the mechanical properties of the active component. Unlike the passive component, which can be measured in the absence of the active component, we can measure the active component only in the presence of the passive component. If we provisionally suppose that k_{sm} is large and k_{pc} is small, then the passive component mainly represents the mechanical contributions of the matrix, and the active component mainly represents the mechanical contributions of the cells. Hence, a perturbation of the FPM, which mainly influences the active component, would be supposed to have mainly affected cytoskeletal structure. Conversely, a perturbation that mainly influenced the passive component would be expected to have mainly influenced the ECM. If a structural change affects both active and passive components, then the effects specific to the cytoskeletons and to the ECM can be extracted only with the aid of a valid quantitative model that relates the structure of an FPM to its mechanics (Zahalak et al., 2000).

The passive component

The mechanical properties of the matrix are profoundly influenced by the remodeling process, which occurs after formation of the collagen gel. During this process the cells compress and stiffen the matrix. The effect of the remodeling process persists even after the cells are largely eliminated from the tissue mechanical system (Fig. 6). As demonstrated in Fig. 10, both the force and stiffness of the matrix as a function of strain are independent of the initial density of cells for densities equal to or greater than 400,000/ml. This is in contrast to the stress and modulus, both of which increase with increasing cell density at corresponding strains (Fig. 14). The change in stiffness is likely to depend not only on the increased density of the collagen filaments in the compressed gel, but also on noncovalent cross-links introduced by the cells (Tranquillo, 1999). Over a period of days to weeks in culture covalent cross-links are formed, which further stiffen the tissue model (Huang et al., 1993). The extent of compression depends on the initial density of cells in the gel (Fig. 11).

Dynamic stiffness

Both the passive and active stiffnesses were observed to increase linearly with the force, at an approximate rate of $0.008\ \mu m^{-1}$. For an elastic material such a linear relation implies an exponential dependence of force on strain. Several natural biological tissues have this behavior (Fung, 1993). The actual value of the passive dynamic stiffness was observed to be higher than the static stiffness, defined as the slope of the passive force-length curve measured in slow ramp stretch. However, the stretch rates used to measure the dynamic stiffness were relatively high, with a frequency approximately equal to the inverse characteristic relaxation time of the matrix (Zahalak et al., 2000), and this may be the reason for the increase in stiffness.

The active component, however, does not behave like an elastic material, because both the stiffness and the force vary linearly with strain. Such behavior is reminiscent of muscle fibers, where a linear variation of force with strain implies a linear variation of stiffness with strain, because both are proportional to the number of myosin molecules (cross-bridges) bonded to actin (Ford et al., 1981). However, the slope of the static force-length curve depends on the rate of increase of bonded cross-bridges with length. Thus, for such actin-myosin contractile systems there is no simple relation between the static and dynamic stiffnesses, as there is for an elastic material, although there is a simple

TABLE 1 Modulus of tissue

Type of tissue	Elastic Modulus (MPa)	Reference
Tendo achillis	375	Lewis and Shaw (1997)
Human knee menisci	73–151 (circumferential)	Tissakht and Ahmed (1995)
Human knee menisci	30–60 (radial)	Tissakht and Ahmed (1995)
Human brachial artery	4	Bank and Kaiser (1998)
Human small artery	0.1–2	Intengan et al. (1999)
FPM*	0.08–0.24	Chapuis and Agache (1992)
Collagen sponge	0.017–0.028	Jain et al. (1990)
FPM	0.8	This work

*0.65 mg/ml collagen, 57,000 cells/ml.

relation between force and dynamic stiffness. The stiffnesses of the passive tendon (Rack and Westbury, 1984) and the active contractile tissue (Joyce and Rack, 1969) have been measured with dynamic length perturbations, for example, for the cat soleus muscle in situ. Both of these stiffnesses increase approximately linearly with force. Scaled to the dimensions of our FPM test specimens, the rate of change of stiffness with force is 0.008 μm^{-1} for tendon and 0.005 μm^{-1} for active contractile tissue. These numbers are close to our experimental values and suggest that contractile interactions may have an important influence on the mechanics of the active component, while quite different dynamics of polymer networks may account for the passive component's behavior. For comparison, the stiffness of passive rabbit papillary muscle also increases linearly with force, but at a rate of only 0.0008 μm^{-1} (Fung, 1993) when scaled to the dimensions of our FPMs.

The dynamic stiffness varies approximately linearly with $\log(\nu)$. This behavior is also seen in biological tissues and has been discussed in terms of a phenomenological model based on a continuous spectrum of relaxation times for the tissue (Fung, 1993). An important problem for the future is to interpret this behavior in terms of defined cell structures and their dynamic mechanical properties.

Comparison of mechanical properties of FPMs with natural tissues

The mechanical parameters obtained from this work are compared to published values in Tables 1–3, except in this work the elastic modulus was obtained from the derivative of the stress-strain relationship. The dependence on strain rate was not characterized. As discussed above, the dynamic stiffness measured at 0.5 Hz was higher than the stiffness obtained for the slope of the stress-strain curves measured at slow stretching speeds. The dynamic elastic modulus of the FPM was around 0.8 MPa at maximum strain. This value is ~5-fold lower than that of the larger arteries but is in the range seen in small arteries. This gap can be minimized by strengthening the ECM and increasing the cell volume occupying the tissue. The FPMs studied here were incubated for only 2 days and cells occupied at most ~12% of the tissue, whereas smooth muscle cells occupied 69% in the small arteries (Intengan et al., 1999).

Supposing that the active component measures cellular elastic properties, the dynamic elastic modulus of the CEF at the maximum strain used in this work (~2.5 MPa) is close to that of single smooth muscle cells, but is three orders of magnitude greater than measured by shearing single CEF between microplates (Thoumine and Ott, 1997). Differences in measurement techniques could be responsible for this discrepancy, but a change of the CEF to a myofibroblast phenotype expressing smooth muscle actin as seen in granulation tissue might also contribute (Grinnell, 1994). Since the single cell measurement is done within a few hours of the attachment of the cell to the microplate, a less organized actin cytoskeleton and focal adhesion complexes might influence stress development (Chrzanowska-Wodnicka and Burridge, 1996). The estimated force production by a single CEF (assuming the average cross-sectional area of the cell is ~50 μm^2) is ~1000 nN, which, apart from the values of Kolodney et al., also measured in

TABLE 2 Modulus of cell

Cell	Elastic Modulus (MPa)	Reference
Single smooth muscle	6.8	Harris and Warshaw (1991)
Single smooth muscle	1.2	Glerum et al. (1990)
Single CEF	0.001	Thoumine and Ott (1997)
CEF	2.5	This work

TABLE 3 Force produced by a single cell

Cell	Force (nN/cell)	Reference
Smooth muscle*†	1500	Harris and Warshaw (1991)
Keratocytes*‡	48	Oliver et al. (1995)
Fibroblasts*§	52	Roy et al. (1999)
Fibroblasts*¶	40	Thoumine and Ott (1997)
Fibroblasts*‖	1–3 (nN/μm^2)	Galbraith and Sheetz (1997)
Fibroblasts**	500	Kolodney and Wysolmerski (1992)
Fibroblasts**	0.1	Eastwood et al. (1996)
Fibroblasts	1000	This work

*Force is measured by a single cell manipulation.
Force is measured by †force transducer, ‡silicon substratum, §collagen substratum, ¶microplates, ‖nano-fabricated substratum.
**Force is estimated from the contractile force produced by FPMs.

FPMs, is much higher than the values listed for fibroblasts in Table 3. This force level is, however, comparable to that measured for smooth muscle cells. Apart from differences dependent on measurement technique, the higher force values measured in FPMs could be due to an enhancement of fibroblast contractility by interactions with ECM proteins, including fibronectin and collagen, which could activate cell contraction via a positive feedback loop as proposed by Schoenwaelder and Burridge (1999).

SUMMARY AND CONCLUSIONS

We have shown that the mechanical properties of reconstituted model connective tissues can be conveniently and simply characterized using the approaches described. Like natural biological tissues, the models show an exponential dependence of force on strain and a linear dependence of dynamics stiffness on $\log(\nu)$. The active and passive mechanical components, obtained by using CD to eliminate the cytoskeletal contributions, were related to the cytoskeletal and ECM structures in the tissue. The intensive mechanical parameters of the active and passive components were calculated separately by measuring the ratio of cell area to the total cross-sectional area of the tissue using confocal microscopy and image reconstruction. FPMs have the advantageous quality of maintaining cells within a relatively natural three-dimensional matrix environment similar to a natural tissue. This approach can be used to assess the mechanical function of cytoskeletal and matrix proteins. For example, the functions of cytoskeletal proteins, which have been eliminated from cells via molecular genetic methods, can be investigated in model tissues assembled from the mutant cells (Eschenhagen et al., 1997; Zutter et al., 1999). Furthermore, this approach can be used to assess and optimize the mechanical properties of reconstituted tissue, an important objective in tissue engineering.

This work was partially supported by National Institutes of Health Grant GM38838.

REFERENCES

Bank, A. J., and D. R. Kaiser. 1998. Smooth muscle relaxation: effects on arterial compliance, distensibility, elastic modulus, and pulse wave velocity. *Hypertension.* 32:356–359.

Barocas, V. H., A. G. Moon, and R. T. Tranquillo. 1995. The fibroblast-populated collagen microsphere assay of cell traction force—Part 2. Measurement of the cell traction parameter. *J. Biomech. Eng.* 117: 161–170.

Bell, E., B. Ivarsson, and C. Merrill. 1979. Production of a tissue-like structure by contraction of collagen lattices by human fibroblasts of different proliferative potential in vitro. *Proc. Natl. Acad. Sci. U.S.A.* 76:1274–1278.

Chapuis, J. F., and P. Agache. 1992. A new technique to study the mechanical properties of collagen lattices. *J. Biomech.* 25:115–120.

Chartier, L., L. L. Rankin, R. E. Allen, Y. Kato, N. Fusetani, H. Karaki, S. Watabe, and D. J. Hartshorne. 1991. Calyculin-A increases the level of protein phosphorylation and changes the shape of 3T3 fibroblasts. *Cell Motil. Cytoskeleton.* 18:26–40.

Chrzanowska-Wodnicka, M., and K. Burridge. 1996. Rho-stimulated contractility drives the formation of stress fibers and focal adhesions. *J. Cell Biol.* 133:1403–1415.

Eastwood, M., R. Porter, U. Khan, G. McGrouther, and R. Brown. 1996. Quantitative analysis of collagen gel contractile forces generated by dermal fibroblasts and the relationship to cell morphology. *J. Cell Physiol.* 166:33–42.

Eriksson, J. E., D. L. Brautigan, R. Vallee, J. Olmsted, H. Fujiki, and R. D. Goldman. 1992. Cytoskeletal integrity in interphase cells requires protein phosphatase activity. *Proc. Natl. Acad. Sci. U.S.A.* 89:11093–11097.

Eschenhagen, T., C. Fink, U. Remmers, H. Scholz, J. Wattchow, J. Weil, W. Zimmermann, H. H. Dohmen, H. Schafer, N. Bishopric, T. Wakatsuki, and E. L. Elson. 1997. Three-dimensional reconstitution of embryonic cardiomyocytes in a collagen matrix: a new heart muscle model system [In Process Citation]. *Faseb J.* 11:683–694.

Ferry, J. D. 1980. Viscoelastic Properties of Polymers. John Wiley, New York.

Findley, W. N., J. S. Lai, and K. Onaran. 1976. Creep and Relaxation of Nonlinear Viscoelastic Materials. Dover Publications, Inc., New York.

Ford, L. E., A. F. Huxley, and R. M. Simmons. 1981. The relation between stiffness and filament overlap in striated frog muscle fibers. *J. Physiol.* 311:219–249.

Fung, Y. C. 1993. Biomechanics. Mechanical Properties of Living Tissues. Springer-Verlag, New York.

Galbraith, C. G., and M. P. Sheetz. 1997:A micromachined device provides a new bend on fibroblast traction forces. *Proc. Natl. Acad. Sci. U.S.A.* 94: 9114–9118.

Glerum, J. J., R. Van Mastrigt, and A. J. Van Koeveringe. 1990. Mechanical properties of mammalian single smooth muscle cells. III. Passive properties of pig detrusor and human a terme uterus cells. *J. Muscle Res. Cell Motil.* 11:453–462.

Goeckeler, Z. M., and R. B. Wysolmerski. 1995. Myosin light chain kinase-regulated endothelial cell contraction: the relationship between isometric tension, actin polymerization, and myosin phosphorylation. *J. Cell Biol.* 130:613–627.

Grinnell, F. 1994. Fibroblasts, myofibroblasts, and wound contraction. *J. Cell Biol.* 124:401–404.

Harris, D. E., and D. M. Warshaw. 1991. Length versus active force relationship in single isolated smooth muscle cells. *Am J. Physiol. Cell Physiol.* 260:C1104–C1112.

Hirano, K., L. Chartier, R. G. Taylor, R. E. Allen, N. Fusetani, H. Karaki, and D. J. Hartshorne. 1992. Changes in the cytoskeleton of 3T3 fibroblasts induced by the phosphatase inhibitor, calyculin-A. *J. Muscle Res. Cell Motil.* 13:341–353.

Huang, D., T. R. Chang, A. Aggarwal, R. C. Lee, and H. P. Ehrlich. 1993. Mechanisms and dynamics of mechanical strengthening in ligament-equivalent fibroblast-populated collagen matrices. *Ann. Biomed. Eng.* 21:289–305.

Intengan, H. D., L. Y. Deng, J. S. Li, and E. L. Schiffrin. 1999. Mechanics and composition of human subcutaneous resistance arteries in essential hypertension. *Hypertension.* 33:569–574.

Jain, M. K., R. A. Berg, and G. P. Tandon. 1990. Mechanical stress and cellular metabolism in living soft tissue composites. *Biomaterials.* 11: 465–472.

Janmey, P. A., U. Euteneuer, P. Traub, and M. Schliwa. 1991. Viscoelastic properties of vimentin compared with other filamentous biopolymer networks. *J. Cell Biol.* 113:155–160.

Joyce, G. C., and P. M. H. Rack. 1969. Isotonic shortening and lengthening movements of cat soleus muscle. *J. Physiol.* 204:475–491.

Kolodney, M. S., and E. L. Elson. 1993. Correlation of myosin light chain phosphorylation with isometric contraction of fibroblasts. *J. Biol. Chem.* 268:23850–23855.

Kolodney, M. S., and E. L. Elson. 1995. Contraction due to microtubule disruption is associated with increased phosphorylation of myosin regulatory light chain. *Proc. Natl. Acad. Sci. U.S.A.* 92:10252–10256.

Kolodney, M. S., and R. B. Wysolmerski. 1992. Isometric contraction by fibroblasts and endothelial cells in tissue culture: a quantitative study. *J. Cell Biol.* 117:73–82.

Lewis, G., and K. M. Shaw. 1997. Tensile properties of human tendo Achillis: effect of donor age and strain rate. *J. Foot Ankle Surg.* 36: 435–445.

Luna, E. J., and A. L. Hitt. 1992. Cytoskeleton-plasma membrane interactions. *Science.* 258:955–964.

Murphy, R. A. 1980. Mechanics of vascular smooth muscle. *In* Handbook of Physiology, Section 2: The Cardiovascular System. D. F. Bohr, A. P. Somlyo, and H. V. Sparks, editors. American Physiological Society, Bethesda, MD. 325–351.

Oliver, T., M. Dembo, and K. Jacobson. 1995. Traction forces in locomoting cells. *Cell Motil. Cytoskeleton.* 31:225–240.

Petersen, N. O., W. B. McConnaughey, and E. L. Elson. 1982. Dependence of locally measured cellular deformability on position on the cell, temperature, and cytochalasin B. *Proc. Natl. Acad. Sci. U.S.A.* 79: 5327–5331.

Rack, P. M. H., and D. R. Westbury. 1984. Elastic properties of the cat soleus tendon and their functional importance. *J. Physiol.*. 347: 479–495.

Roy, P., W. M. Petroll, H. D. Cavanagh, and J. V. Jester. 1999. Exertion of tractional force requires the coordinated up-regulation of cell contractility and adhesion. *Cell Motil. Cytoskeleton.* 43:23–34.

Satoh, H., L. M. Delbridge, L. A. Blatter, and D. M. Bers. 1996. Surface-volume relationship in cardiac myocytes studied with confocal microscopy and membrane capacitance measurements: species-dependence and developmental effects. *Biophys. J.* 70:1494–1504.

Schoenwaelder, S. M., and K. Burridge. 1999. Bidirectional signaling between the cytoskeleton and integrins. *Curr. Opin. Cell Biol.* 11: 274–286.

Schor, S. L. 1980. Cell proliferation and migration on collagen substrata in vitro. *J. Cell Sci.* 41:159–175.

Stopak, D., and A. K. Harris. 1982. Connective tissue morphogenesis by fibroblast traction. I. Tissue culture observations. *Dev. Biol.* 90:383–398.

Thoumine, O., and A. Ott. 1997. Time scale dependent viscoelastic and contractile regimes in fibroblasts probed by microplate manipulation. *J. Cell Sci.* 110:2109–2116.

Tissakht, M., and A. M. Ahmed. 1995. Tensile stress-strain characteristics of the human meniscal material. *J. Biomech.* 28:411–422.

Tranquillo, R. T. 1999. Self-organization of tissue-equivalents: the nature and role of contact guidance. *Biochem. Soc. Symp.* 65:27–42.

Zahalak, G. I., J. E. Wagenseil, T. Wakatsuki, and E. L. Elson. 2000. A cell-based constitutive relation for bio-artificial tissues. *Biophys. J.* 79: 2369–2381.

Zutter, M. M., S. A. Santoro, J. E. Wu, T. Wakatsuki, S. K. Dickeson, and E. L. Elson. 1999. Collagen receptor control of epithelial morphogenesis and cell cycle progression. *Am. J. Pathol.* 155:927–940.